PROC. OF JSCE,
No. 241, SEPT. 1975

TURBULENCE OF OPEN CHANNEL FLOW OVER SMOOTH AND ROUGH BEDS

By Hiroji NAKAGAWA, Iehisa NEZU** and Hiroshi UEDA****

1. INTRODUCTION

In the last decade a broad knowledge of dynamics of wall turbulence in water flow has been obtained through development of a hot-film anemometer or a hydrogen-bubble method. One of the headmost studies in this field was done by a group of Stanford University[1] under the direction of Kline who looked for the mechanism of turbulence production by means of flow visualization with the hydrogen-bubble method. Several experimental works done by use of both flow visualization and point measurements have recently brought to light turbulence characteristics of the shear flow, with aid of improved methods of data analysis.

Turbulence measurments of open-channel shear flow over a smooth or rough bed were vigorously done by Raichlen[2], McQuivey et al.[3], Ishii et al.[4] and Imamoto[5] by making use of single-sensor hot-film anemometer.

It is very interesting in practice to investigate how the structure of turbulence would be influenced by hydraulic parameters such as Reynolds number and Froude number of the mean flow and the wall parameter represented by equivalent roughness. To this end a systematic measurement of turbulent open-channel flow over smooth and rough beds has been done by making use of single- and dual-sensor hot-film anemometers in order to make clear the dynamics of turbulence from a viewpoint of energy budget, and subsequently the conventional formulae on the mean velocity distribution have been discussed in consideration of turbulence structures.

2. METHODS OF EXPERIMENT AND DATA ANALYSIS

The tests described in Table 1 were made in a tilting flume 0.5 m wide and 15 m long. The bed roughness was made by spreading the spherical glass beads with uniform diameter all over the bed. Since Reynolds number ($Re=U_m h/\nu$, U_m: the mean velocity, h: the flow depth) and Froude number ($Fr=U_m/\sqrt{gh}$) are nearly constant on an average for all runs, it may be expected to appreciate only the effect of roughness.

A DISA type 55A89 dual-sensor hot-film anemometer was used to measure the spatial components of instantaneous velocities in a major portion of the flow, and in a part close to the wall a single-sensor hot-film anemometer of DISA type 55A83 was used to supplement the data.

Table 1 Hydraulic data for experiments

Case	h (cm)	Aspect ratio B/h	U_{max} (cm/s)	U_m (cm/s)	U_* (cm/s)	U_*' (cm/s)	$\frac{\lvert U_*-U_*'\rvert}{U_*}$ (%)	$Re=\frac{U_m h/\nu}{\times 10^4}$	$Fr=U_m/\sqrt{gh}$	Slope S $\times 10^{-4}$	Q (l/s)	$k_s^*=U_* k_s/\nu$	h/k_s	T_w (°C)
A-1	7.77	6.43	16.83	14.80	0.810	0.780	3.8	1.09	0.170	0.80	5.75	0	∞	18.35
B-1	7.94	6.29	17.69	15.45	0.895	0.938	4.8	0.98	0.175	1.13	6.14	9.1	62.1	11.35
C-1	7.88	6.34	15.69	13.22	0.989	0.999	1.0	0.98	0.150	1.23	5.21	48.0	15.3	17.95
D-1	7.63	6.55	17.21	13.87	1.336	1.416	5.6	0.86	0.160	2.77	5.29	136.2	6.1	12.30

U_*: from Log-Law, $U_*'=\sqrt{ghS}$, Q: Discharge, T_w: Water Temperature

* Dr. Eng., Professor, Dept. of Civil Engineering, Kyoto University.
** M.S.C.E., Graduate Student, Dept. of Civil Engineering, Kyoto University.
*** M.S.C.E., A Technical Official, 4th District Port Construction Bureau, The Ministry of Transportation.

To diminish the effects of variation of water temperature and the impurities included in water upon the radiative characteristics of the hot-film as much as possible, a stable temperature of water was kept by circulating water all day long before a test began, and the floating materials were filtered by gauzes. The hot-film anemometers were calibrated by means of both a Pitot tube and a float before and after at each run[6].

The velocity measurements recorded in the magnetic tapes were converted into the digital quantities and then analyzed in a statistical way by using a large electronic computer, Data Processing Center, Kyoto University. For certain reasons of spectrum analysis, 2,100 samples with 0.01 sec. time interval for each record were mainly chosen.

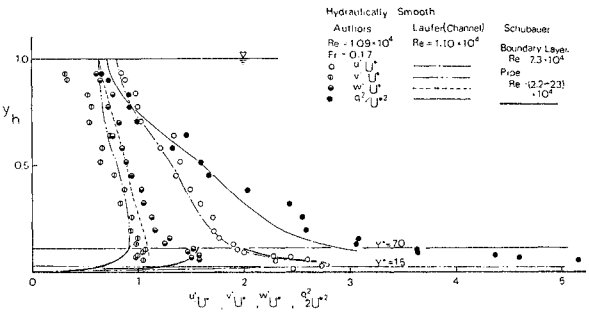

Fig. 1 Turbulence intensities over smooth bed.

3. EXPERIMENTAL RESULTS

(1) The Mean Velocity Distribution and the Friction Velocity

Let x, y and z be the longitudinal coordinate in the flow direction, the vertical coordinate to the wall ($y=0$ corresponds to the wall), and the spanwise coordinate parallel to the wall, respectively. U, V and W denote the components of the mean velocity, u, v and w the components of velocity fluctuation, and u', v' and w' the values of rms amplitude.

Now, in order to measure the mean velocity U the preliminary test was conducted by making use of Pitot tube and it was shown that the flow along the center line of the channel was nearly two-dimensional, normal and fully-developed turbulent. The velocity distribution of the mean flow over a smooth bed agrees well with Nikuradse's curve[26], while for the flow over a rough bed an origin of the y-axis needs to be shifted to a point $k_s/4$ below the top of the sphere so as to get agreement with Nikuradse's curve. The friction velocity U_* for each run obtained by putting the plotted data on Nikuradse's curve is compared with the values given by $U_*'=\sqrt{ghS}$ (S: bed slope) in Table 1, and both values show a good agreement.

(2) The Distribution of Turbulence Intensity

In Fig. 1 the dimensionless distributions of turbulence intensities u', v', w' and of turbulent energy $q^2/2$ (where, $q^2=u'^2+v'^2+w'^2$) for the flow over a smooth bed are shown together with Laufer's data on turbulent flow in closed channel[7]. As to u'/U_* the authors' data agree well with Laufer's curve and indicate the maximum value 2.8 at $y^+(=yU_*/\nu)\simeq 15$ as Schubauer[8] certified for the inner layer in the boundary-layer and pipe flows. The values of w'/U_* near the wall and of v'/U_* near the free surface deviate from Laufer's results. Because the fluid motion in y-direction is restrained by free surface, v' near the free surface may become smaller than that in pipe flow. All of the test on both smooth and rough beds show the fact that $u'>w'>v'$. Because this relationship can be derived from the turbulent energy budget[9] and turbulent eddy model[10], too, it must be applicable to any kinds of wall turbulence.

The turbulent flow over a rough bed showed nearly same characteristics of turbulence intensity as those over a smooth bed[11]. However, as the effect of roughness appears with increase of k_s^+ ($=k_sU_*/\nu$), the variation of turbulence intensities near the wall becomes flatter, while at the point far away from the wall, the intensities are independent of roughness. Grass[12] and Chen et al.[18] found the similar characteristics that turbulence intensity u'/U_* in the wall region gradually decreased with enlargement of k_s^+. The observed data of u', v' and w' in the wall region are compared for some kinds of roughness in Fig. 2. The values of u'/U_* gradually decrease with increase of k_s^+, but v'/U_* and w'/U_* are hardly influenced by size of roughness element. u' has a direct relation to large-scale eddies which dominate the turbulence production[9].

Though the turbulence production in the flow over a smooth bed occurs mostly in a buffer-layer of $y^+=10$-30 by burst or sweep due to the flow instability[1], a buffer-layer over a rough bed disappears perfectly or partly into roughness elements and consequently, turbulence would be produced in another way. A poor dependence of v'/U_* and w'/U_* on roughness may be due to

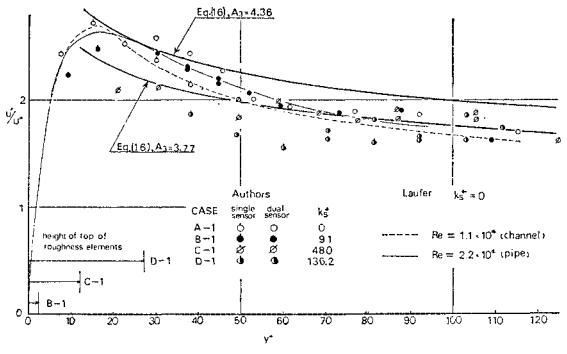

(a)

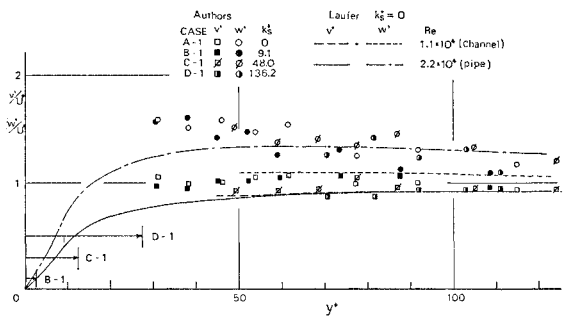

(b)

Fig. 2 Turbulence intensities in wall region.

their little contribution to turbulence production, so that both v' and w' change monotonously with y^+ while u' shows the maximum value.

On considering that turbulence intensity near the wall can be represented by an universal function of y^+ as described by Monin et al.[14], it is questionable that only the values of w' are so variable according to Re in Fig. 2 and so Laufer's data may be unreliable. This might cause the difference among the values of w' in Fig. 1, but the details should be discussed further.

(3) The Distribution of Reynolds Stress

The observed values of dimensionless Reynolds stress $-\overline{uv}/U_*^2$ are plotted in Fig. 3, together with the following theoretical expression derived from the equation of motion:

$$-\frac{\overline{uv}}{U_*^2}=(1-\xi)-\frac{1}{\kappa R_*\xi} \quad \cdots\cdots(1)$$

where $\xi=y/h$, $R_*=hU_*/\nu$, $\kappa=0.4$ (Kármán constant) and a logarithmic law of the velocity distribution on the mean flow is assumed (cf. **3.** (1)). Since the value of R_* is 600 to 900 in this case, the viscous term in Eq. (1) is negligible for larger value of ξ and consequently Reynolds stress varies linearly with ξ.

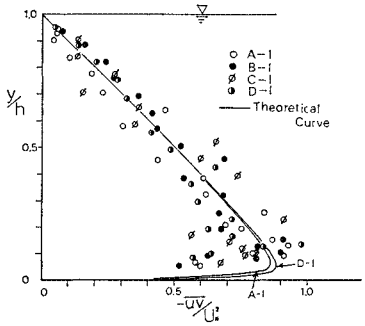

Fig. 3 Reynolds shear stress.

The observed data nearly satisfy Eq. (1) except a region close to the wall. However, according to Antonia et al.[15] the measurement of Reynolds stress in the neighborhood of wall shows lower accuracy than the one of turbulence intensity, and it is affected by the velocity gradient and the non-uniformity of calibration factors. Then, more accurate data are needed to discuss further.

(4) Spectrum Distribution

At present the space spectra can be estimated only by applying Taylor's hypothesis of the frozen turbulence to the time spectra obtained by direct measurement. Because this hypothesis is fairly reasonable in the range $kL_x \gg 1$ where wave number k is much larger than a reciprocal of the mean eddy size L_x as indicated by Lin[16], the time spectrum obtained by F.F.T. method was transformed into the space power spectrum on the basis of Taylor's hypothesis, and then it was normalized into the one-dimensional wave spectrum $S(k)$ by dividing by its turbulence intensity. In this case $S(k)$ satisfies the following:

$$\int_0^\infty S(k)dk \fallingdotseq \int_0^{k_\infty} S(k)dk=1 \quad \cdots\cdots(2)$$

where k_∞ is the maximum wave number possible to be analyzed.

By the fact that the observed space spectra nearly satisfy Eq. (2) within a few percentages of the error, it can be concluded that $S(k)$ estimated above gives a fairly reasonable expression. Data of $S(k)$ for different sampling intervals observed at a definite point over a smooth bed are plotted in Fig. 4, and the similar tendency of $S(k)$ against k has been certified for other measuring points. For turbulent flow over a rough bed $S(k)$ has shown nearly same distribution as over a smooth bed.

Now, it is still debatable whether turbulence

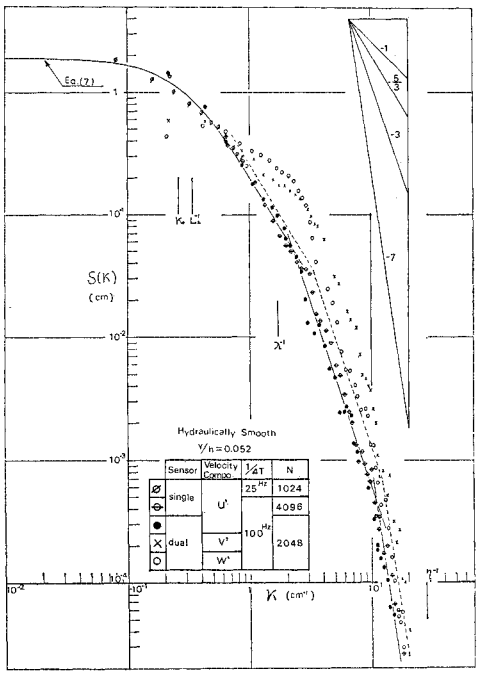

Fig. 4 An example of normalized spectra.

should be treated as a lump of 'wave' or of 'eddy'. But when 'wave' is characterized by wave number k and 'eddy' by its size l, it is concluded that $k\sim l^{-1}$ and so the wave spectrum $S_u(k)$ of u'^2 can be divided into three subranges corresponding to eddy size as follows:

(a) Productive subrange (large-scale eddy)

Because the length scale in this case is of order of the mean eddy size L_x, $L_x k_0\sim 1$ is satisfied for a characteristic wave number k_0. Since L_x is of the same order as the mean flow, there would be surely a strong interaction between the eddies and the mean flow, resulting in production of turbulent energy. $S_u(k)$ satisfies the -1 power law owing to this interaction[17], and for $k\ll k_0$ it shows nearly constant value due to aliasing effect.

(b) Viscous subrange (small-scale eddy)

The characteristic length is of very small scale which is given by the Taylor microscale λ ($=\sqrt{15\nu u'^2/\epsilon}$) or the Kolmogoroff microscale η ($=(\nu^3/\epsilon)^{1/4}$). ϵ is the dissipation rate of turbulent energy defined by

$$\epsilon=\frac{\nu}{2}\overline{\left(\frac{\partial u_i}{\partial x_j}+\frac{\partial u_j}{\partial x_i}\right)^2}\geq 0. \quad \cdots\cdots(3)$$

An example of the dissipation spectrum $D_u(k)=k^2S_u(k)$ is shown in Fig. 5, in which $D_u(k)$ indicates its peak at $k\sim\lambda^{-1}$ and reduces considerably at $k\sim\eta^{-1}$. Now,

$$\lambda^{-2}\simeq\lambda_x^{-2}=\int_0^\infty D_u(k)dk. \quad \cdots\cdots(4)$$

Refering to Fig. 5 and Eq. (4) the viscous subrange may be divided into two stages: one is the initial stage of a large dissipation scale at which the -3 power law of $S_u(k)$ is applicable[18] and another is the final stage of a small dissipation scale at which the -7 power law is valid[19].

(c) Inertial subrange (intermediate-scale eddy)

The relationship between eddy sizes in ranges

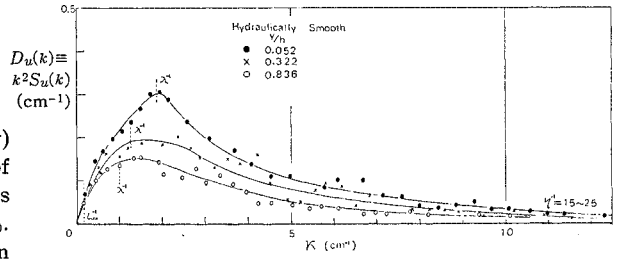

$D_u(k)\equiv k^2S_u(k)$ (cm^{-1})

Fig. 5 Energy dissipative spectral functions.

Table 2 Spectral density functions

Subrange	Productive subrange		Inertial subrange	Viscous subrange	
				Initial	Final
Wave number	$0\leq k\ll k_0$	$k\sim k_0\sim L_x^{-1}$	$L_x^{-1}\ll k\ll\lambda^{-1}$	$k\sim\lambda^{-1}$	$k\sim\eta^{-1}$
One-dimensional spectral function $u'^2S_u(k)$	$\frac{2}{\pi}L_xu'^2$	$\sim(\epsilon/k_0)^{2/3}k^{-1}$ (by Tchen)	$C\epsilon^{2/3}k^{-5/3}$ (by Kolmogoroff)	$\sim(\epsilon/\nu)k^{-3}$ (by Inoue)	$\sim(\epsilon/\nu^2)^2k^{-7}$ (by Heisenberg)
Interpolated formula $u'^2S_u(k)$	$\frac{2}{\pi}L_xu'^2(1+(k/k_0)^2)^{-5/6}$ (Kármán's formula)				
			$C\epsilon^{2/3}k^{-5/3}(1+\gamma(k\lambda)^2)^{-2/3}$ $\gamma=$Const.$\times R_*^{-1/2}$		
			$C\epsilon^{2/3}k^{-5/3}(1+\gamma'(k\eta)^4)^{-4/3}$ (Heisenberg's formula)		γ': Const.

(a) and (b) is written by

$$L_x/\lambda \sim (1/4)R_*^{1/2}, \qquad \lambda/\eta \sim 4R_*^{1/4}. \quad \cdots\cdots(5)$$

When Reynolds number R_* is enough large so that $L_x \gg \lambda$, there is an intermediate subrange between (a) and (b) ranges, where the energy cascade process occurs and the $-5/3$ power law is valid[19];

$$u'^2 S_u(k) = C\epsilon^{2/3}k^{-5/3} \quad \text{(by Kolmogoroff)}. \quad \cdots\cdots(6)$$

The above results are summarized in Table 2, together with the formula interpolated between two ranges. Although a definite inertial range cannot be appreciated on account of relatively small values of R_* in authors' tests, Bradshow[20] has pointed out that Eq. (6) is approximately valid even when range (c) overlaps with a part of range (a) or (b) if the interaction with each range is feeble. In fact a range where the $-5/3$ power law is valid has been recognized here as shown in Fig. 4.

Presence of the productive and viscous subranges as indicated in Table 2 is certified by Fig. 4, though the latter may be doubtful because of poor analytical capacity of the measuring devices. Since $S_u(k)$ in productive and inertial ranges contributes mainly to turbulence intensity, the interpolated formula by Kármán may be available in these ranges:

$$S_u(k) = \frac{2}{\pi} L_x \{1+(k/k_0)^2\}^{-5/6}. \quad \cdots\cdots(7)$$

Eq. (7) agrees fairly well with the observed data in both ranges (Fig. 4).

As to $S(k)$ of v'^2 and w'^2 ($S_v(k)$ and $S_w(k)$) both indicate almost same characteristics, which agree well with Laufer's experimental results. Since v' and w' do not directly contribute to turbulence production as previously mentioned, the productive range of these components will be so scarcely expected that $S(k)$ for a large-scale eddy shows more gradual variation with k and may be the peak in this range due to aliasing effect[9]. $S(k)$ for a small-scale eddy computed by introducing a relation[19] of isotropic turbulence into equations in Table 2 is given by a dotted line in Fig. 4. Isotropy can be recognized in the viscous subrange.

(5) Dissipation of Turbulent Energy

The dissipation rate of turbulence is an essential quantity for dynamics of turbulence. The dissipation of energy ϵ is represented by Eq. (3), but most of the terms cannot be measured by convenient means. Thus ϵ should be evaluated

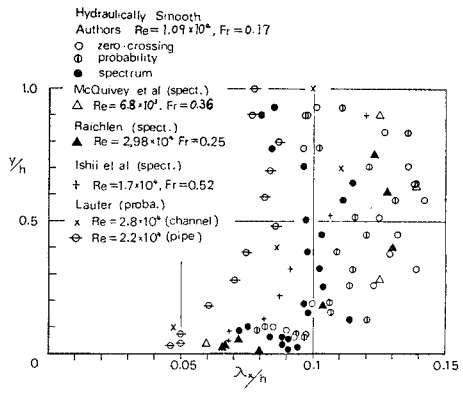

Fig. 6 Taylor microscale over smooth bed.

by using the isotropic relation more or less.

Since the small-scale structure of turbulence is approximated to be isotropic, the dissipation rate is given[7] by

$$\epsilon = 15\nu u'^2/\lambda_x^2. \quad \cdots\cdots(8)$$

λ_x can be evaluated from the spectrum given by Eq. (4) or the probability distribution of $\partial u/\partial x$ or the zero-crossing method on the assumption that u and $\partial u/\partial x$ have normal distributions[24]. The vertical distributions of λ_x on a smooth bed obtained by these methods are shown in Fig. 6, together with other researchers' data. In spite of dependence of λ_x upon R_*, λ_x/h tends to become smaller toward the free surface and the wall, and its mean value is of order of 0.1. Since it is recognized from Fig. 5 that the spectral method may give the most reliable results, λ_x obtained by this method is adopted here.

Now, when λ_y and λ_z are computed from such relations as $\lambda_y^{-2} = \int_0^\infty k^2 S_v(k)dk/2$ and then the isotropic approximation is applied to Eq. (3), the dissipation rate may be written as

$$\epsilon = 5\nu q^2/\lambda'^2, \qquad \lambda' = \frac{1}{3}(\lambda_x+\lambda_y+\lambda_z). \quad \cdots\cdots(9)$$

Even supposing Eq. (9) affords more accurate value of ϵ than Eq. (8), the results are subject to the effects of noise in higher frequency range and of the uncertainty of the isotropic assumption.

If an inertial subrange for $S_u(k)$ exists, Eq. (6) should be used to obtain the dissipation rate, as indicated by Grant et al.[22] and Lawn[23]. Referring to Bradshaw's study[20], the universal constant C in Eq. (6) is expected to be about 0.5 even at comparatively small Reynolds numbers at which authors' experiment has conducted. The estimating error of ϵ by making use of

Eq. (6) is at most 15 percentages for $C=0.5\pm 0.05$ and smaller than that caused by Eq. (3)[20].

The dissipation rates evaluated from Eqs. (6), (8) and (9) are compared in Fig. 7 (a) as well as data for a smooth bed given by other investigators[7),23),25]. The fact that Eq. (8) leads to larger values of ϵ than Eq. (6) in a core region away from the bed may be due to non-isotropy of turbulence[24].

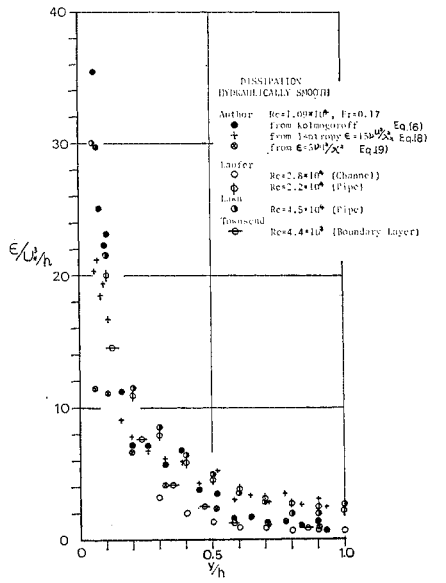

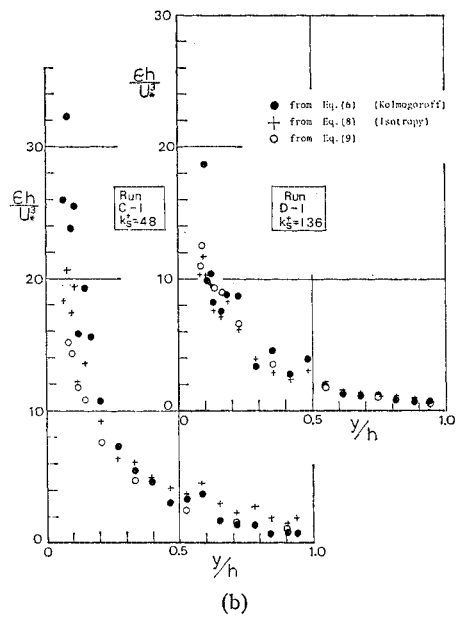

Fig. 7 Comparison of energy dissipation determined by various methods.

Turbulent flow on a rough bed exhibits similar characteristics of dissipation as that on a smooth bed, but with increase of roughness better closeness between the results obtained by Eq. (6) and ones by Eq. (8) has been recognized, as shown in Fig. 7 (b). This means that the turbulent flow over a rough bed shows more remarkable tendency to isotropy. In physical sense turbulent energy of the flow on a rough bed is redistributed more rapidly than on a smooth bed, consequently attaining isotropic structure. The dissipation rates $\epsilon h/U_*^3$ for all runs evaluated by Eq. (6) are plotted in Fig. 8. In spite of slight dispersion in observed data, it may be possible to express them by an universal function independently of Reynolds number and property of the wall.

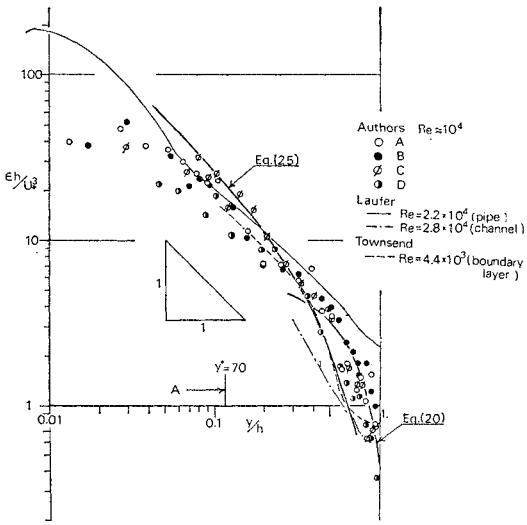

Fig. 8 Energy dissipation under various flow conditions.

For ξ below about 0.5 except the range very close to the wall, the difference of the dissipation rate between open-channel, pipe and boundary-layer flows is hardly recognized, but for ξ above about 0.5 ϵ in open-channel flow becomes larger than that in boundary layer flow and smaller than that in pipe flow, consequently depending much upon the boundary conditions of the mean flow. Its difference may be caused by existence of free surface and asymmetry of the flow field in open-channel flow.

(6) Production and Transport of Turbulent Energy

The turbulence production P is written as

$-\overline{uv}\partial U/\partial y$ and thus easily obtained if Reynolds stress and mean velocity distributions are determined. On applying the logarithmic law to the mean velocity, the theoretical production rate of turbulence can be given by

$$Ph/U_*^3=\left(1-\xi-\frac{1}{\kappa R_*\xi}\right)\Big/\kappa\xi\,. \quad \cdots\cdots(10)$$

The experimental values of turbulence production are compared with Eq. (10) for smooth and rough beds in Fig. 10 (a) and (b), respectively. A good agreement between the observed values and the theoretical ones can be shown for small range of R_*, not depending upon the property of the wall.

The transport rate of kinetic energy T is defined as

$$T\equiv\frac{\partial}{\partial y}\frac{\overline{(u'^2+v'^2+w'^2)v}}{2}=\frac{\partial}{\partial y}\left(\frac{\overline{q^2v}}{2}\right) \quad \cdots\cdots(11)$$

Though the correlations between v and w are not measured here, the experimental data about the transport rate are shown in Fig. 9 on the assumption that $\overline{q^2v}/2=\overline{(u^2/2+v^2)v}$, because it is concluded by Laufer[7] that $\overline{vw^2}\simeq\overline{vv^2}$ regardless of Reynolds number.

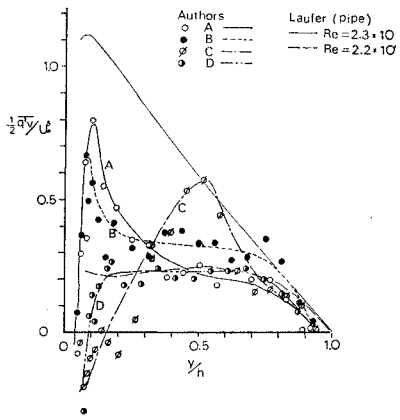

Fig. 9 Turbulent energy transport.

With increase of the roughness size the variation of $\overline{q^2v}/2U_*^3$ becomes slower and its peak appears further away from the wall, taking smaller value. This tendency can be inferred from the fact that the kinetic energy of the flow over a smooth bed varies more rapidly with ξ than that over a rough bed[11]. However, for ξ larger than 0.6 the turbulence transport is hardly influenced by the scale of roughness.

Anyway, the transport rate which contains the triple correlations of fluctuating velocity ought to be discussed on the basis of the measurements with the higher accuracy. As long as the observed data presented by authors are not of the highest order of accuracy, the conclusion described above should be appreciated only qualitatively.

(7) The Turbulent Energy Budget

It was pointed out at early stage of turbulence research that the turbulent energy budget should be clarified in order to argue the structure of turbulence[25]. The equation of turbulent energy in a two-dimensional turbulent shear flow can be written, provided that the Reynolds number of the flow is very large and the work done by the viscosity can be neglected, by

$$P=\epsilon+T+R \quad \cdots\cdots(12)$$

where R is the transport rate of the pressure energy defined as $R=\partial/\partial y\cdot(\overline{pv}/\rho)$. Because it is very difficult to obtain the correlation between the pressure p and the velocity v by direct measurement, R may be evaluated from Eq. (12) by making use of P, ϵ and T previously obtained. As mentioned above the observed values of T are not so accurate that R cannot be evaluated precisely too, and consequently only a qualitative description about the transport of the pressure energy will be presented here.

Well, the turbulent energy budget over a smooth bed is shown in Fig. 10 (a). It indicates the similar characteristics as Laufer's results about the pipe flow[7]. In the buffer layer ($y^+<30$ according to Laufer) P, ϵ, T and R are of same order so that P is approximately balanced by ϵ, and T by $-R$. In the range $\xi<0.7$ beyond the buffer layer the transport of kinetic energy T plays only secondary role in the turbulence behaviours and is nearly balanced by the transport of pressure energy R. Since for $\xi>0.7$ the turbulence production and the pressure transport are scarcely recognized, the dissipation rate is nearly balanced by the transport of kinetic energy.

From above investigations into turbulence behaviours it is concluded that the energy excess range where $P>\epsilon$ exists near the wall while the energy deficiency range where $\epsilon>P\simeq0$ exists near the free surface. Between two ranges there exists the intermediate range where the energy flows under a dynamically equilibrium state so that $P\simeq\epsilon$. And this structure is similar to the energy flow in the space spectrum expressed by wave number. On the other, the pressure transport can be noticed to occur only near the wall.

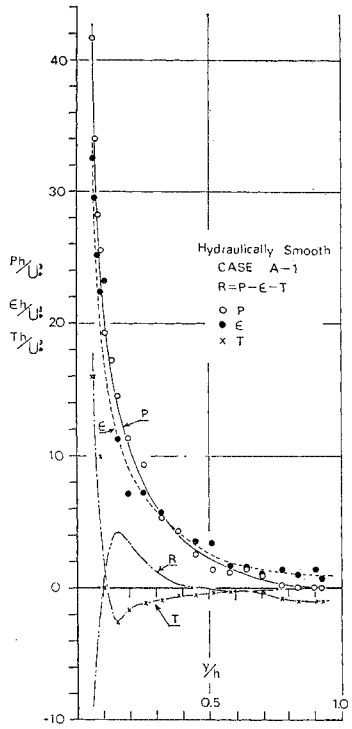

(a) Turbulent energy budget over smooth bed.

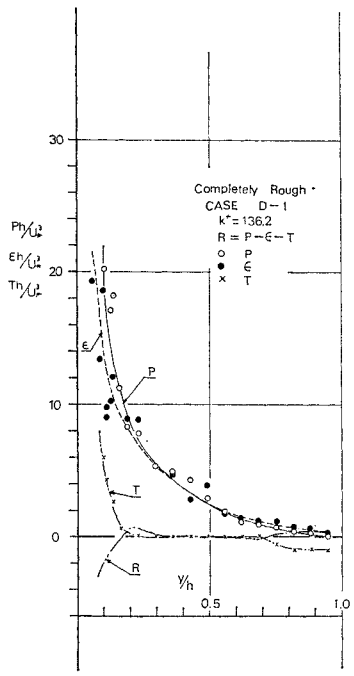

(b) Turbulent energy budget over rough bed.

Fig. 10

On considering the sign of R, the pressure energy is transported toward the wall in opposition to the kinetic energy, resulting in disturbances in a viscous sublayer.

As to the turbulent flow over a rough bed the point which the kinetic energy changes from a loss to a gain, that is $T=0$, shifts further away from the wall and the pressure transport to balance to the kinetic energy transport also occurs in wider range with increase of the roughness as shown in Fig. 10 (b). The turbulence transport as well as turbulence intensity u' and kinetic energy $q^2/2$ may be influenced by the roughness scale, as mentioned previously.

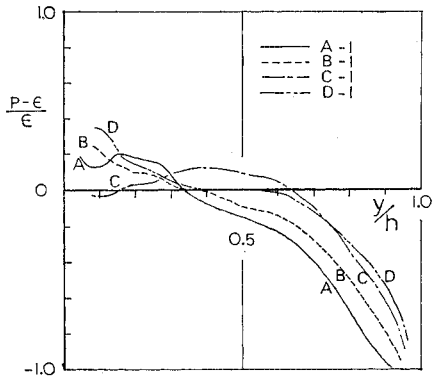

Fig. 11 Relationship between production and dissipation.

As already expected, the turbulence production indicates almost same characteristics as the turbulence dissipation and both of them balance nearly in the whole depth except in the neighbourhood of water surface, regardless of properties of the wall. This relationship between P and ϵ for each run is shown in Fig. 11, and it can be concluded that an equilibrium state of turbulence under which $P \cong \epsilon$ appears in longer distance from the wall as the wall boundary becomes rougher.

4. INVESTIGATION INTO VELOCITY DISTRIBUTIONS OF MEAN MOTION

(1) Division of Turbulent Flow Field

As pointed out by Tennekes et al.[9], there is an evident similarity between the spatial and

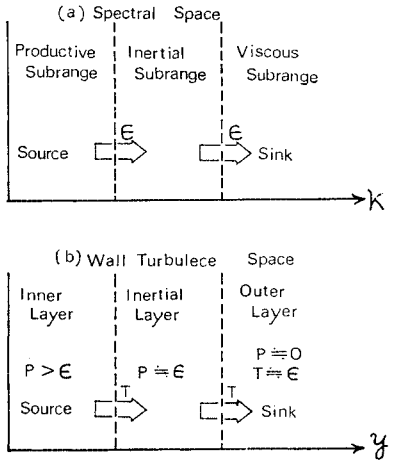

Fig. 12 Analogy between spectral space and wall turbulence space.

spectral structures of wall turbulence. At very large Reynolds number the spectral space (wave number space) is divided into three subranges as shown in Fig. 12 (a) and the corresponding spatial structure is shown in Fig. 12 (b). Because the turbulent energy produced in inner layer is larger than the dissipation rate, the excess energy is transported toward an upper layer. In outer layer corresponding to a viscous subrange the production hardly occurs and the dissipation is cancelled by the energy transport from an inner layer. Between both layers there exists inertial layer in which the production rate is nearly equal to the dissipation, and it corresponds to an inertial subrange in the spectral space.

The above mentioned means that there exists a qualitative similarity between the spatial and spectral structures. Their quantitative structures are obviously to be different each other. Especially, since the wave number k has a reciprocal relation to the distance y, the length scales in both spaces have a quite inverse relation in size.

Such a division of turbulent flow field in open-channel is shown in Fig. 13. The characteristics in each region are:

1) *Wall region* In this region corresponding to 'inner layer' in boundary layer flow, the scales of characteristic length and velocity are ν/U_* and U_*, respectively, and the law of the wall is valid. The conspicuous production of turbulence is come out due to burst and sweep. This is the most important region for wall turbulence.

2) *Free surface region* In this region corresponding to 'outer layer' the length and velocity scales are h and the maximum velocity U_{max}, respectively, and the velocity defect law is valid. This is apt to be influenced by the free surface in open-channel flow.

3) *Equilibrium region* This is an intermediate region between the wall region and the free surface one, in which a dynamically equilibrium state for turbulent energy budget, that is $P \cong \epsilon$, is realized. It corresponds to the inertial subrange where a similarity of turbulence structure is valid[19], and the characteristic length and velocity scales are y and $\sqrt{\tau/\rho}$, respectively.

Now, on giving an universal expression by length and velocity scales to the characteristic quantities of turbulence, it comes into question what kind of basic quantity should be chosen. In consideration of similarity between the turbulent field and the wave number space, the dissipation rate ϵ can be taken here. Since the most reliable quantity through turbulence measurements is the intensity u', ϵ is related to u' by using Eq. (2). Because $S(k)$ given by Eq. (7) is valid in a range of wave number which contributes quite mainly to u'^2, the relationship between ϵ and u' can be written from Eq. (6) for $C=0.5$:

$$u'/U_* = 1.131(\epsilon L_x/U_*^3)^{1/3} . \quad \cdots\cdots\cdots\cdots(13)$$

The mean eddy size L_x in Eq. (13) was evaluated as $(2/\pi)S(0)$ by joining $S(k)$ to a correlation function by Fourier transformation. However, as it is questionable to apply Taylor's hypothesis of the frozen turbulent flow to a range with low wave number, L_x above obtained is to be considerably approximate value.

The observed values of L_x are indicated in Fig. 14. Owing to deficiency of the data close to the wall for run D, it is difficult to get a definite conclusion about the effect of roughness, but it is not too much to say from Fig. 14 that the values of L_x/h decrease with increase of

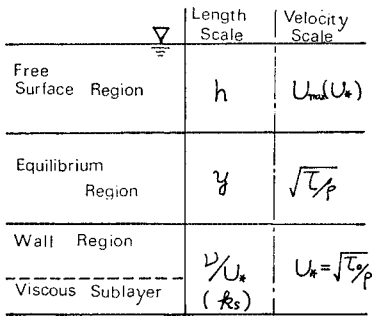

Fig. 13 Subregions in open channel flow.

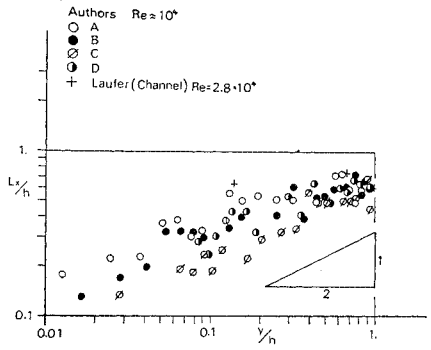

Fig. 14 Mean eddy scale (Macroscale).

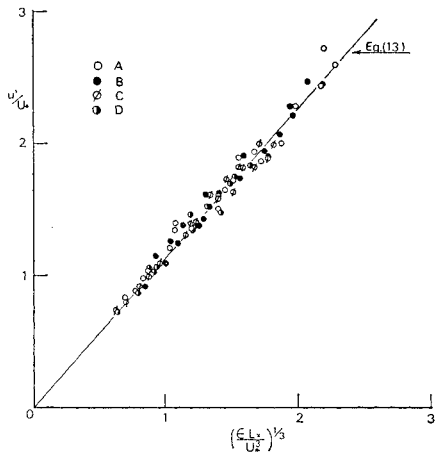

Fig. 15 Verification of applicability of Kármán's formula.

roughness. Chen[13] et al. and Antonia[15] et al. also pointed out that the mean eddy size decreased with enlargement of roughness element. It may be caused that the large-scale eddies near the wall are forced by the roughness elements to break up into a wake. Validity of Eq. (13) is examined in comparison with the experimental values in Fig. 15, and it is rather surprising that the observed values fairly agree with Eq. (13) on considering the low accuracy of measurement of L_x. From this result it can be concluded that the spectral distribution in the productive and the inertial subranges satisfies Kármán's equation given by Eq. (7) and that analysis of the measurements has remarkably high accuracy.

Well, taking account of Eq. (13) as a basic relation in turbulence and of existence of three regions, the turbulence characteristics and the mean velocity distribution in each region are discussed below from a viewpoint of turbulent energy budget.

(2) Wall Region ($y^+ \lesssim 100$)

The conventional researches[26] on the mean velocity distribution revealed that the characteristic length scale in this region is ν/U_* for hydraulically smooth and k_s for completely rough and depends upon both scales for incompletely rough. However, on considering great difficulty to solve the dynamics of turbulent flow with different multi-scales[9] and the lack of accurate measurements of turbulence in the wall region for rough bed, all the data obtained here are consistently arranged by ν/U_*, regardless of the bed property.

The observed values of ϵ are shown in Fig. 16, dimensionlessly formed by the characteristic scales, ν/U_* and U_*. These show a fixed distribution independent of the type of roughness. The peak of dissipation appears at $y^+=10\sim20$, and so the buffer-layer corresponding to $y^+=10\sim30$ may play an important role on dynamics of turbulence in the wall region. Although the peak value obtained by the authors is about one half of Laufer's one, for $y^+>30$ a good agreement between both results has been recognized. Consequently, its universal expression can be given by

$$\epsilon\nu/U_*^4 = A_1(y^+)^{-1} \quad \cdots\cdots(14)$$

where A_1 is an universal constant.

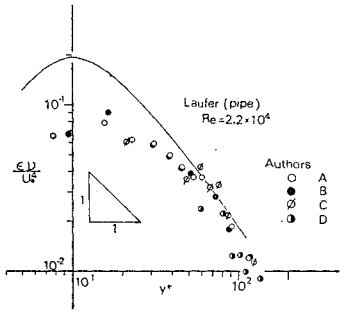

Fig. 16 Energy dissipation in wall region.

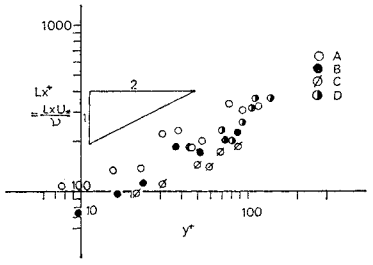

Fig. 17 Mean eddy scale in wall region.

The experimental values of the mean eddy size in the wall region L_x are plotted in Fig. 17 and can be approximately represented by

$$L_x^+ \equiv L_x U_*/\nu = A_2(y^+)^{1/2} \quad \cdots\cdots(15)$$

where A_2 obviously depends upon the type of the wall so as to decrease with increase of roughness. Substitution of Eqs. (14) and (15) into Eq. (13) yields

$$u'/U_* = A_3(y^+)^{-1/6}, \qquad A_3 \equiv 1.131(A_1A_2)^{1/3}. \quad \cdots\cdots(16)$$

Though the values of A_1 and A_2 should be determined by a vast amount of measurements, A_1 becomes about 1.85, A_2 about 31 for run A (smooth), and A_2 about 20 for run C (rough), and consequently A_3 becomes about 4.4 and 3.8 for smooth and rough beds, respectively, within authors' experiments. As shown in Fig. 2 (a) the curves representing Eq. (16) may coincide well with the experimental values for $y^+>30$. When an eddy scale decreases with increase of the roughness size, u'/U_* tends to decrease due to redistribution of turbulent energy, and isotropic tendency develops as mentioned previously.

Next, by introducing a mixing length l^+ between two large-scale eddies, the following relation will be obtained:

$$u'/U_* \sim l^+ \frac{\partial(U/U_*)}{\partial y^+}. \quad \cdots\cdots(17)$$

Since Prandtl's hypothesis that the mixing length for an eddy scale of order L_x^+ is proportional to y^+ may be valid in this region, the mean velocity can be represented as, by combining Eqs. (16) and (17),

$$U/U_* = A_4\{A_5 - (y^+)^{-1/6}\}. \quad \cdots\cdots(18)$$

On the other hand, for $30<y^+<100$ u'/U_* can be regarded to be nearly constant as shown in Fig. 2 (a) and consequently the equation of the mean velocity becomes

$$U/U_* = (1/\kappa)\ln y^+ + A_6. \quad \cdots\cdots(19)$$

From the velocity gradient of Eqs. (18) and (19), $\kappa A_4 = 6(y^+)^{1/6} \fallingdotseq 11.4$, and so A_4 is nearly an universal constant. But, it is understood that the value of A_5 as well as A_6 should be a function of the roughness which must be determined from many experiments as done by Nikuradse[26].

Now, substituting $\kappa=0.4$, $A_4=28.4$, $A_5=1.06$ and $A_6=5.5$ for smooth bed into Eqs. (18) and (19), the theoretical distribution curves are shown in Fig. 18 together with the experimental values. A fairly good agreement between the theoretical formulae and the observed values has been obtained, and Eqs. (18) and (19) coincide each other

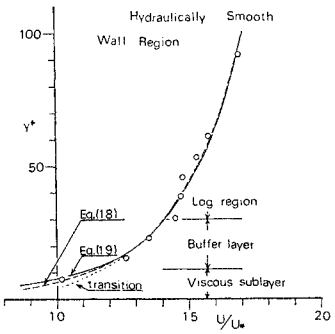

Fig. 18 Mean velocity distribution in wall region.

for $y^+>15$ so perfectly that Prandtl's equation approved as the law of the wall is well valid in this region because a slight variation of u'/U_* scarcely acts upon the mean velocity distribution. From the above investigation it may be concluded that characteristic length scale ν/U_* is valid even for a rough bed to discuss the turbulence structures in wall region.

(3) Free Surface Region ($0.6\leq\xi\leq1.0$)

The dynamics of turbulent flow in this region which occupies the principal part of the mean flow depends upon the flow parameters such as Reynolds number and Froude number which characterize the flow field as a whole. Therefore the characteristic length and velocity scales are h and U_{max}, respectively. Since U_{max} can be related to U_* for specified wall roughness, U_* is chosen as the velocity scale instead of U_{max} here. And ξ' $(=1-\xi)$ is taken as a dimensionless ordinate. This region reveals a turbulence characteristic that the energy production hardly occurs so that the dissipation rate is almost equal to the transport rate.

Well, despite of a little scattering of the observed values, the following equation can be approximately derived from Fig. 8.

$$\epsilon h/U_*^3 = 4(\xi'+0.1). \quad \cdots\cdots(20)$$

And, regarding L_x/h in this region as nearly constant to be equal to 0.58 independently of the roughness size as shown in Fig. 14, Eq. (13) becomes

$$u'/U_* = 1.5(\xi'+0.1)^{1/3}. \quad \cdots\cdots(21)$$

This is shown in Fig. 19 and has a good agreement with the observed values for $0\leq\xi'<0.5$.

Although it is considerably difficult to evaluate the transport rate, the following relationship can be obtained by Zagustin's hypothesis[27] that the turbulence transport occurs due to the difference

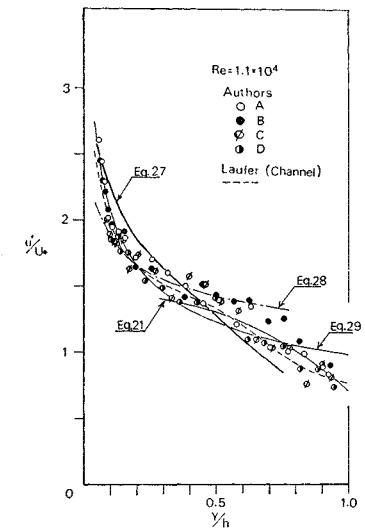

Fig. 19 Turbulence intensity of u'.

of the mixing length l between two adjacent eddies and that its intensity is proportional to the gradient of l, that is $1/2(\overline{q^2v})\sim U_*^3\partial l/\partial y$, in consideration of $T\simeq\epsilon$ in this region, and by using Eq. (20);

$$\frac{d^2(l/h)}{d\xi'^2}=-B_1(\xi'+0.1)\,. \quad \cdots\cdots(22)$$

Integration of Eq. (22) yields

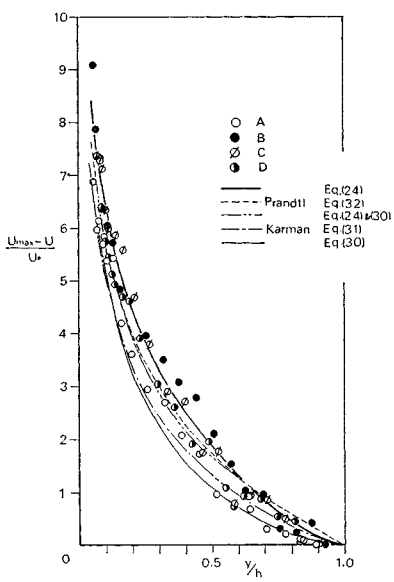

Fig. 20 Mean velocity distribution in free surface region and equilibrium region.

$$\frac{l}{h}=\frac{\kappa}{3}\cdot\left\{(1-\xi'^3)+\frac{1}{12}(1-\xi')^2(1+2\xi')\right\}. \quad \cdots\cdots(23)$$

Now, substituting Eqs. (1) and (23) into the relation $d(U/U_*)/d\xi'=-\sqrt{\tau/\tau_0}\,/(l/h)$ given by the mixing length theory and integrating it, the mean velocity distribution can be obtained for small values of ξ':

$$\frac{U_{max}-U}{U_*}=\frac{2}{\kappa}\left\{\tanh^{-1}\xi'^{3/2}+\frac{\xi'^{3/2}}{8(\xi'+1)}\right\}. \quad \cdots\cdots(24)$$

Since the second term on right hand side of Eq. (24) is only as large as eight percentages of the first term, Zagustin's formula which ignores the former may be enough available. According to Nikuradse[26] $l/h=0.14$ at $\xi'=0$ and so κ becomes 0.39 from Eq. (23). Eq. (24) computed with this value is shown in Fig. 20. The observed values may deviate a bit from Eq. (24) by influence of the free surface, but an approximate coincidence between both can be recognized in this region so that the velocity defect law is valid independently of the wall roughness.

(4) Equilibrium Region ($0.1\leq\xi\leq0.6$)

If it is tentatively assumed that the equilibrium state of turbulence is obtained under the condition $|P-\epsilon|/\epsilon\leq20\%$, the equilibrium region may be defined as $0.1<\xi<0.6$ from Fig. 11. The turbulence characteristics in this region are so little influenced by the external conditions that similarity of turbulence is valid, resulting in an universal function expressed by the characteristic scales y and $\sqrt{\tau/\rho}$ [25]. Then,

$$\frac{\epsilon h}{U_*^3}=C_1\frac{(1-\xi)^{3/2}}{\xi}\,. \quad \cdots\cdots(25)$$

Eq. (25) for $C_1=3.0$ is shown in Fig. 8 and nearly agrees with the observed data, while Luafer's results can be expressed by

$$\epsilon h/U_*^3=C_2(1/\xi) \quad \cdots\cdots(26)$$

which corresponds to the velocity scale U_* instead of $\sqrt{\tau/\rho}$.

It is recognized from Fig. 14 that L_x/h is proportional to $\xi^{1/2}$ in this region and thus Eq. (13) can be rewritten, by making use of Eq. (25), as

$$u'/U_*=C_3(1-\xi)^{1/2}\xi^{-1/6}\,. \quad \cdots\cdots(27)$$

Eq. (27) may not show a good agreement with the observed data as shown in Fig. 19, and it seems better to use Eq. (26) in consideration of variation of L_x, that is,

$$u'/U_*\sim\xi^{-1/6}(L_x/h\sim\xi^{1/2}) \quad \cdots\cdots(28)$$

$$u'/U_*\sim\xi^{-1/3}(L_x/h\sim\text{const.}) \quad \cdots\cdots(29)$$

where L_x/h is considered to vary with $\xi^{1/2}$ at the first stage of this region and to reach nearly constant value at the middle as found in Fig. 14. u'/U_* seems to take an intermediate value between Eqs. (28) and (29).

Now, $P=-\overline{uv}(\partial U/\partial y)\simeq\epsilon$ in this region and, integrating it by using Eqs. (1) and (25), the mean velocity distribution can be given by

$$\frac{U_{max}-U}{U_*} = -C_1[2\{\ln(1-\sqrt{1-\xi})+\sqrt{1-\xi}\}-\ln\xi]. \quad \cdots\cdots(30)$$

On the other hand Kármán[26] applied a hypothesis of similarity to the equation of motion by taking l and $\sqrt{\tau/\rho}$ as the characteristic scales and obtained the following:

$$\frac{U_{max}-U}{U_*}=-\frac{1}{\kappa}\{\ln(1-\sqrt{1-\xi})+\sqrt{1-\xi}\}. \quad \cdots\cdots(31)$$

And, an extension of Eq. (19) into this region yields

$$\frac{U_{max}-U}{U_*}=-\frac{1}{\kappa}\ln\xi. \quad \cdots\cdots(32)$$

Since Eq. (30) is deduced by averaging Eqs. (31) and (32) weighted with a ratio of 2 to -1, it may be supposed that this region overlaps to some extent with the wall region. When C_1 is equal to 3.0 as given by this experiment, κ becomes 0.33 which is nearly 0.4. Eqs. (30), (31) and (32) are shown in Fig. 20. As expected, Eq. (30) coincides well with Eq. (31) based on Kármán's hypothesis but becomes smaller than the observed values. This is because the boundary condition in Eq. (30) has been given at $\xi=1$. Now, Eq. (30) agrees with them fairly well when the curve is connected smoothly with Eq. (24). However, the differences among all of the theoretical mean velocity are below U_* that is of the same order of turbulence intensity. For the practical purposes any of distribution curves will be able to be used in the whole range except very close to the wall.

5. CONCLUSION

In this paper turbulence measurements in open channel shear flow by making use of a single- and a dual-sensor hot-film anemometers have been described. The effects of bed roughness on structures of wall turbulence have been mainly investigated by keeping Reynolds number and Froude number nearly constant.

It has been recognized that the mean eddy size and the intensity u' decrease with increase of roughness, and consequently it is inferred that redistribution of turbulent energy in the flow over a rough bed may develop more rapidly than over a smooth one, so as to approach to isotropic state.

The flow field has been divided into three regions on the basis of a close analogy between the wave number space and the turbulent flow field. Then, the velocity distributions of the mean flow in each region have been deduced from the viewpoint of turbulent energy budget and discussed in comparison with the existing formulae.

Although a lot of knowledge about turbulence in open channel flow have been obtained here, the dynamics of turbulence in the wall region which is the most complicated and interesting remains to be solved because of insufficient measurements, and it should be examined further together with the mechanism of turbulence generation.

ACKNOWLEDGEMENTS

The authors wish to express deep graduates to Messrs. A. Kimura, Assistant of Kyoto University, and T. Tamezawa, a graduate student of Kyoto University, for their kind helps in analyzing the data.

BIBLIOGRAPHIES

1) Kline, S. T., Reynolds, W. C., Schraub, F. A. and Rundtadler, P. W.: The structure of turbulent boundary layers, Jour. of Fluid Mech., Vol. 30, 1967, pp. 741-773.
2) Raichlen, F.: Some turbulence measurements in water, Proc. of ASCE, EM-2, 1967, pp. 73-97.
3) McQuivey, R. S. and Richardson, E. V.: Some turbulence measurements in open-channel flow, Proc. of ASCE, HY-1, 1969, pp. 209-223.
4) Ishii, S., Itakura, T. and Kishi, T.: Turbulence measurements in open-channel flow by hot-film anemometer, Proc. of JSCE, No. 180, 1970, pp. 51-60 (in Japanese).
5) Imamoto, H.: Hydraulic studies on turbulence in open-channel flow, Doctral thesis presented to Kyoto University, 1971 (in Japanese).
6) Nakagawa, H., Nezu, I. and Ueda, H.: Turbulence measurements in pipe flow by a

dual-sensor hot-film anemometer, Proc. of Annual Meeting of Kansai Branch of JSCE, 1973 (in Japanese).
7) Laufer, J.: The structure of turbulence in fully developed pipe flow, TR-1174, NACA, 1954.
8) Schubauer, G. B.: Turbulent processes as observed in boundary layer and pipe, Jour. of Applied Physics, Vol. 25, 1954, pp. 188-196.
9) Tennekes, H. and Lumley, J. L.: A first course in turbulence, The M.I.T. Press, 1972.
10) Nakagawa, H. and Nezu, I.: On a new eddy model in turbulent shear flow, Proc. of JSCE, No. 231, 1974, pp. 61-70.
11) Nakagawa, H., Nezu, I. and Ueda, H.: Turbulence characteristics in open-channel flow over smooth and rough surfaces, Proc. of Annual Meeting of JSCE, II-181, 1974 (in Japanese).
12) Grass, A. J.: Structural features of turbulent flow over smooth and rough boundaries, Jour. of Fluid Mech., Vol. 50, 1971, pp. 233-255.
13) Chen, C. K. and Roberson, J. A.: Turbulence in wakes of roughness elements, Proc. of ASCE, HY-1, 1974, pp. 53-67.
14) Monin, A. S. and Yaglom, A. M.: Statistical fluid mechanics; Mechanics of turbulence, The M.I.T. Press, 1971, pp. 257-416.
15) Antonia, R. A. and Luxton, R. E.: The response of a turbulent boundary layer to a step change in surface roughness, Jour. of Fluid Mech., Vol. 48, 1971, pp. 721-761.
16) Lin, C. C.: On Taylor's hypothesis and the acceleration terms in the Navier-Stokes equations, Quar. of Applied Math., Vol. X, 1953, pp. 295-306.
17) Tchen, C. M.: On the spectrum of energy in turbulent shear flow, Jour. of R.N.B.S., Vol. 50, 1953, pp. 51-62.
18) Inoue, E.: On the structure of wind near the ground, Bull. of the National Institute of Agricultural Sciences, Ser. A, No. 2, 1952.
19) Batchelor, G. K.: Homogeneous turbulence, Cambridge Univ. Press, 1953.
20) Bradshaw, P.: Conditions for the existence of an inertial subrange in turbulent flow, N.P.L., R&M, No. 3603, 1967.
21) Kármán, T.: Progress in the statistical theory of turbulence, Proc. of N.A.S., Vol. 34, 1948, pp. 530-539.
22) Grant, H. L., Stewart, R. W. and Moilliet, A.: Turbulence spectra from a tidal channel, Jour. of Fluid Mech., Vol. 12, 1962, pp. 241-268.
23) Lawn, C. J.: The determination of the rate of dissipation in turbulent pipe flow, Jour. of Fluid Mech., Vol. 48, 1971, pp. 477-505.
24) Laufer, J.: Investigation of turbulent flow in a two-dimensional channel, TR-1053, NACA, 1951.
25) Townsend, A. A.: The structure of turbulent shear flow, Cambridge Univ. Press, 1956.
26) Schlichting, H.: Boundary layer theory, McGraw-Hill, 1968, pp. 560-625.
27) Zagustin, A. and Zagustin, K.: Analytical solution for turbulent flow in pipes, La Houille Blanche, No. 2, 1969, pp. 113-118.

(*Received Dec. 13, 1964*)

コンクリートライブラリー一覧

No.	編著者	題目	定価	〒
3	委員会編	異形鉄筋を用いた鉄筋コンクリート構造物の設計例		
10	委員会編	構造用軽量骨材シンポジウム	500	140
11	樋口芳朗	微細な空げきてん充のためのセメント注入における混和材料に関する研究	120	60
15	委員会編	ディビダーク工法設計施工指針（案）改版	900	210
17	委員会編	MDC 工法設計施工指針（案）	700	210
20	委員会編	フライアッシュを混和したコンクリートの中性化と鉄筋の発錆に関する長期研究	500	100
21	委員会編	バウル・レオンハルト工法設計施工指針（案）	700	210
22	委員会編	レオバ工法設計施工指針（案）	700	140
23	委員会編	BBRV 工法設計施工指針（案）	900	210
24	委員会編	第2回構造用軽量骨材シンポジウム	1100	210
25	丸安・小林 阪本	高炉セメントコンクリートの研究	550	210
26	松本嘉司	鉄道橋としての鉄筋コンクリート斜角げたの設計に関する研究	200	80
27	岡村甫	高張力異形鉄筋の使用に関する基礎的研究	200	60
28	尾坂芳夫	コンクリートの品質管理に関する基礎研究	200	60
29	委員会編	フレシネー工法設計施工指針（案）		
30	委員会編	フープコーン工法設計施工指針（案）	1000	210
31	委員会編	OSPA 工法設計施工指針（案）	1100	210
32	委員会編	OBC 工法設計施工指針（案）	1100	210
33	委員会編	VSL 工法設計施工指針（案）	1000	210
34	委員会編	鉄筋コンクリート終局強度理論の参考	1600	210
35	委員会編	アルミナセメントコンクリートに関するシンポジウム	1300	210
36	委員会編	SEEE 工法設計施工指針（案）	1300	210

37	委員会編	コンクリート標準示方書（昭和49年度版）改訂資料	1500	210
38	委員会編	コンクリートの品質管理試験方法	1500	210
39	委員会編	膨張性セメント混和材を用いたコンクリートに関するシンポジウム	1500	210
40	委員会編	太径鉄筋 D51 を用いる鉄筋コンクリート構造物の設計指針（案）	1650	210